Available online at www.sciencedirect.com
SCIENCE DIRECT®
International Journal of Fatigue 26 (2004) 59–70
International Journal of Fatigue
www.elsevier.com/locate/ijfatigue

In-situ observations of high cycle fatigue mechanisms in cast AM60B magnesium in vacuum and water vapor environments

Ken Gall [a,*], Gerhard Biallas [b], Hans J. Maier [b], Phil Gullett [c], Mark F. Horstemeyer [c], David L. McDowell [d], Jinghong Fan [e]

[a] *Department of Mechanical Engineering, University of Colorado, Boulder, CO 80309, USA*
[b] *Lehrstuhl für Werkstoffkunde (Materials Science), University of Paderborn, 33095 Paderborn, Germany*
[c] *Sandia National Laboratories, Livermore, CA 94550, USA*
[d] *George Woodruff School of Mechanical Engineering, Georgia Institute of Technology, Atlanta, GA 30332, USA*
[e] *Alfred University, NY, USA*

Received 19 December 2002; received in revised form 8 March 2003; accepted 28 March 2003

Abstract

We present in situ scanning electron microscopy (SEM) observations regarding the formation and propagation of small fatigue cracks in cast AM60B magnesium. Using an environmental SEM, observations were made in vacuum and in the presence of water vapor at 20 Torr. In the vacuum environment, fatigue cracks in the magnesium formed preferentially at pores, sometimes precluded by observable cyclic slip accumulation. At higher cycle numbers in the vacuum environment, additional cracks were discovered to initiate at persistent slip bands within relatively large magnesium dendrite cells. The propagation behavior of small fatigue cracks ($a < 6$–10 dendrite cells) was found to depend strongly on both environment and microstructure. Small fatigue cracks in the magnesium cycled under vacuum were discovered to propagate along interdendritic regions, along crystallographic planes, and through the dendrite cells. The preference to choose a given path is driven by the presence of microporosity, persistent slip bands, and slip incompatibilities between adjacent dendrite cells. Fatigue cracks formed more rapidly at certain locations in the water vapor environment compared to the vacuum environment, leading to a smaller total number of cracks in the water vapor environment. The majority of small cracks in magnesium cycled in the water vapor environment propagated straight through the dendrite cells, at a faster rate than the cracks in the vacuum. In the water vapor environment, cracks were observed to grow less frequently through interdendritic regions, even in the presence of microporosity, and cracks did not grow via persistent slip bands. The propagation behavior of slightly larger fatigue cracks ($a > 6$–10 dendrite cells) was found to be Mode I-dominated in both environments.

1. Introduction

Ongoing interest in the use of cast magnesium (Mg) alloys in the auto industry [1,2] has recently triggered substantial research effort focused on the structural properties of this metal. The very low density (1.8 g/cm^3), excellent castability, and easy machinability of Mg [2] make it a strong candidate for intricate lightweight components. One drawback of Mg-based castings is their sensitivity to various urban and industrial environments [3,4]. However, recent studies have linked the corrosion mechanisms in cast Mg to the microstructure, indicating that significant potential exists to improve their performance in corrosive environments [5–7]. Alternatively, coatings for Mg [8,9] may be used to eliminate surface reactions and circumvent corrosion altogether. In parallel with these fundamental studies to model and prevent corrosion in cast Mg, it is necessary to examine the fatigue behavior of this class of materials. In the absence of corrosion, fatigue inevitably emerges as the dominant failure mode for Mg castings under cyclic loading conditions.

Compared to other lightweight wrought and cast materials such as aluminum and titanium alloys, very little work has been performed to characterize the fatigue mechanisms operating in cast Mg alloys. Initial studies examined the low and high cycle fatigue of cast Mg

* Corresponding author. Tel.: +1-303-735-2711; fax: +1-303-492-3498.
E-mail address: kenneth.gall@colorado.edu (K. Gall).

0142-1123/$ - see front matter © 2003 Elsevier Ltd. All rights reserved.
doi:10.1016/S0142-1123(03)00079-3

alloys to determine parameters for traditional fatigue life prediction methodologies [10–12]. The authors in [10–12] concluded that traditional fatigue life prediction tools were sometimes inaccurate for cast Mg alloys. Fatigue crack growth studies have shown that the propagation behavior of large fatigue cracks in Mg is strongly dependent on the environment [13,14]. Higher humidity environments have a tendency to reduce fatigue crack growth thresholds and increase fatigue crack growth rates. More recent studies have begun to examine the relationship between the microstructure and fatigue mechanisms in cast Mg alloys [15–18]. As observed in other cast materials, several studies have linked the formation of fatigue cracks in cast Mg to large pores [15–17]. In addition, several preliminary efforts have related the fatigue crack growth behavior to the microstructure of cast Mg using fracture surface observations [17] or specimen replication techniques [18]. Although preliminary studies have uncovered the basic microstructural aspects of the fatigue of cast Mg alloys, they have not provided detailed information on the mechanisms of crack formation and small crack propagation. In order to successfully develop microstructure- and mechanism-based models of fatigue in cast Mg alloys, it is imperative to understand these early stages of fatigue.

In the present paper we employ in situ fatigue tests conducted in a scanning electron microscope equipped with a small-scale load frame (in situ SEM) to examine the early stages of the fatigue process in cast AM60B Mg. The SEM has an environmental chamber and is capable of imaging at various humidity levels. Here we compare fatigue mechanisms in cast magnesium observed in a vacuum and under water vapor at 20 Torr. We focus on the formation and growth of small fatigue cracks within the microstructure in these different environments. Previous investigators [19–23] have demonstrated that in situ SEM is a useful tool for investigating the behavior of small fatigue cracks. One drawback of earlier in situ SEM studies has been the limitations imposed by the high vacuum required for imaging. With the advent of environmental SEM a few years ago, this is no longer an issue. In principle, it is possible to determine quantitative aspects of formation and growth behavior such as cycles to initiation, growth rates, and crack opening levels. However, in this paper we will focus on qualitative observations of operative crack formation and small crack growth mechanisms. Future investigations will consider quantitative aspects of formation and growth, although the present observations are sufficient to motivate initial micro-mechanical fatigue models for better quantification of the relevant phenomena.

2. Materials and experimental methods

A plate of AM60B magnesium with dimensions of 10 cm by 15 cm by 3 mm was cast in a permanent mold by high-pressure die-casting. The nominal composition of AM60B Mg is provided in Table 1. Flat dog-bone shaped specimens with a 8 mm gage length and a 3 mm by 1–2 mm gage cross section were machined from the plate at various spatial locations. Results will be presented here from in situ tests on two specimens from similar regions of the plate where there is low overall porosity due to high cooling rates. One of the samples was cycled in high vacuum while the other sample was cycled in water vapor at 20 Torr. A third specimen was also extracted from a low porosity region to determine yield and tensile strength under monotonic loading. Numerous other samples have been tested to develop appropriate visualization parameters for in situ fatigue testing of Mg. In addition, several different samples were tested to verify the generality of the present observations. Samples cycled under identical conditions all showed the same qualitative behaviors reported here.

In order to minimize the area that needs to be inspected during testing, small stress concentrations were employed in order to elevate the stresses and favor crack formation in a local region. One stress raiser, used in both fatigue samples, was a dimple with a 3 mm diameter and 120 μm maximum depth placed in the center of the specimen using a dimple grinder which produces low residual stresses. A small spot weld placed in the center of the dimple was used as an additional stress raiser in the sample to be cycled in the vacuum environment. In the sample with the spot weld, cracks were still observed to form away from the artificial defect. Clearly, this indicates that microstructural heterogeneities such as pores cause severe stress concentrations, and/or exist at locations with diminished material fatigue resistance. It should be made clear that the stress concentration in the sample cycled in high vacuum (dimple plus spot weld) was more severe than the stress concentration in the sample cycled in water vapor (dimple).

For in situ observation, the surface of the Mg samples must be polished to successfully detect and track small-scale fatigue damage. A mild etching procedure, either during or after polishing, can be used to remove polishing-induced artifacts and highlight the cast Mg microstructure. However, overetching of the cast Mg results in a deep microstructure that is unsuitable for in situ observations. Due to the reactivity of Mg, numerous attempts were made to achieve the optimal surface for in situ observations. The optimal preparation was achieved by first grinding with a 4000 grit (5 μm) SiC abrasive and a 1:3 glycerine-ethanol solution. The sample was then subsequently polished with a series of 3 and 1 μm diamond pastes with excessive lubricant. The final polish was performed with a SiO_2 suspension (OPS), which

Table 1
Chemical composition of AM60B Mg alloy. Values in weight percent

Mg	Al	Mn	Si	Zn	Fe	Cu	Ni	Other
Bal.	5.5-6.5	0.25 Min	0.10 Max	0.22 Max	0.005 Max	0.010 Max	0.002 Max	0.003 Max (total)

serves as a combined mechanical polishing and chemical etching solution.

Mechanical tests were performed using a small-scale load frame fixed within an environmental SEM. The load frame has a maximum load capacity of 10 kN and a displacement range of 50 mm. The SEM was operated at an accelerating voltage of 20 kV and with two different environments during fatigue testing (a) a relatively high vacuum of $p < 10^{-3}$ Pa (7.4×10^{-6} Torr) and (b) water vapor at 2.7×10^{3} Pa (20 Torr). The water vapor at 20 Torr corresponds to 100% relative humidity at ambient room temperature conditions. Local chemical composition was determined with Energy Dispersive X-ray (EDX) analysis. In situ tests conducted in the SEM do not provide significantly more resolution as compared to other techniques such as replica methods [18], but allow both EDX analysis and imaging using backscattered electrons that can provide additional microstructural information. Completely reversed ($R = \sigma_{min}/\sigma_{max} = -1$) fatigue tests were performed at a displacement rate of 20 μm/s. Gross tensile and compressive load limits were imposed and the machine was programmed to reverse the loading at these limits. The tensile test was performed at a displacement rate of 0.5 μm/s until complete fracture of the specimen. The yield and tensile strengths of the AM60B specimen machined from a low porosity region were measured to be 150 and 285 MPa, respectively.

At the maximum displacement rate, the machine is capable of applying approximately 5000 cycles per day, so a fatigue test lasting 10^6 cycles would take 200 days. In order to accelerate the fatigue process and enhance the possibility of multiple crack formation sites, a nominal cyclic stress amplitude of 135 MPa (Amplitude 1) was applied until the first cracks could be detected. At this amplitude, the first cracks could be observed after preloading to 100 and 130 cycles in water vapor and high-vacuum environments, respectively. Following this pre-cycling, the nominal stress amplitude was decreased to 90 MPa (Amplitude 2) and kept constant during further cycling. We should mention that the pre-cycling procedure at higher amplitude will elevate local cyclic plastic strain levels, which may influence the fatigue processes operating at the subsequent lower amplitude. Extensive SEM observations were made in irregular intervals depending on the progression of fatigue damage. All SEM imaging was performed at the maximum tensile load to accentuate crack opening. The holds were conducted in displacement control, and a minimal amount of stress relaxation (1–2% of max stress) occurred during the hold. In all images presented here, the loading axis is vertical on the page.

3. Experimental results

The undeformed microstructure of the cast AM60B Mg is shown in Fig. 1. For this image the material has been deeply etched to highlight different material phases and the dendritic structure. The slightly blurry appearance of the surface is an artifact of the deep etching and the enhanced contribution of backscattered electrons to the overall signal used to better reveal the microstructure. As highlighted in Fig. 1, and confirmed by local

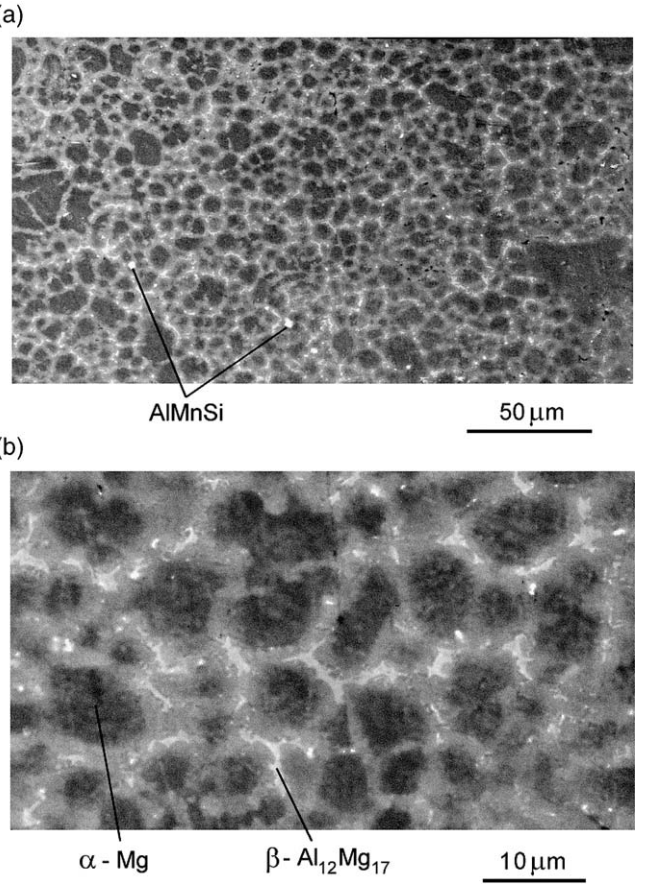

Fig. 1. SEM image of the undeformed microstructure in AM60 Mg at (a) low and (b) high magnification. Phases are identified in the main text.

EDX measurements, three different phases are present in the AM60B microstructure. In Fig. 1a, two AlMnSi particles are indicated. The AlMnSi particles are dispersed throughout the microstructure and they appear brightest on the SEM micrographs due to their elevated position on the surface. A higher magnification image in Fig. 1b, shows the next brightest phase, β-$Al_{12}Mg_{17}$, which occurs in the form of particles decorating the interdendritic regions. The darkest phase is the HCP α-Mg dendrite cells, which contain only trace amounts of Al, and are preferentially polished and etched (Fig. 1b). The interdendritic regions are revealed by the brightness contrast between the β and α phases. In these regions, the Al content was found to be greater than in the α phase but less than in the β phase. The average dendrite cell size (DCS) in the material is approximately 10 microns.

Fig. 2 shows the fracture surfaces of samples cycled (a) in vacuum and (b) in water vapor. The dimple and the spot weld are visible on the sample cycled in vacuum (Fig. 2a), while only the dimple is present in the sample cycled in water vapor (Fig. 2b). The dimple is observed as the gradual rounding of the specimen on the bottom of the fracture surface in Fig. 2a and b. In situ observations were made at several locations on the surface of the samples during cycling. As indicated in Fig. 2, several of the observed locations contained cracks that ultimately linked with the final fracture path. In the sample that was cycled in a vacuum, two regions of observation are distinguished, Region 1 and Region 2. In the sample that was cycled in water vapor, a region of observation is labeled as Region 3. Several observations will be presented from other regions of the sample that did not ultimately link with the final crack that created the fracture surface. The lives of the samples cycled in vacuum and water vapor environments were 35,541 and 14,970 cycles, respectively. These numbers are not meant for direct quantitative comparison since the stress concentration in the sample cycled in vacuum was more severe than the stress concentration in the sample cycled in water vapor. However, the longer life of the sample cycled in vacuum, despite the larger stress concentration, does show that the environment has a considerable influence on the fatigue life.

Figs. 3–5 present observations of the formation of fatigue cracks away from the spot-weld during cycling of the sample at 90 MPa in the vacuum environment. After 3200 cycles at 90 MPa (plus the pre-cycling at 135 MPa), the first cracks appeared near larger pores. In Fig.

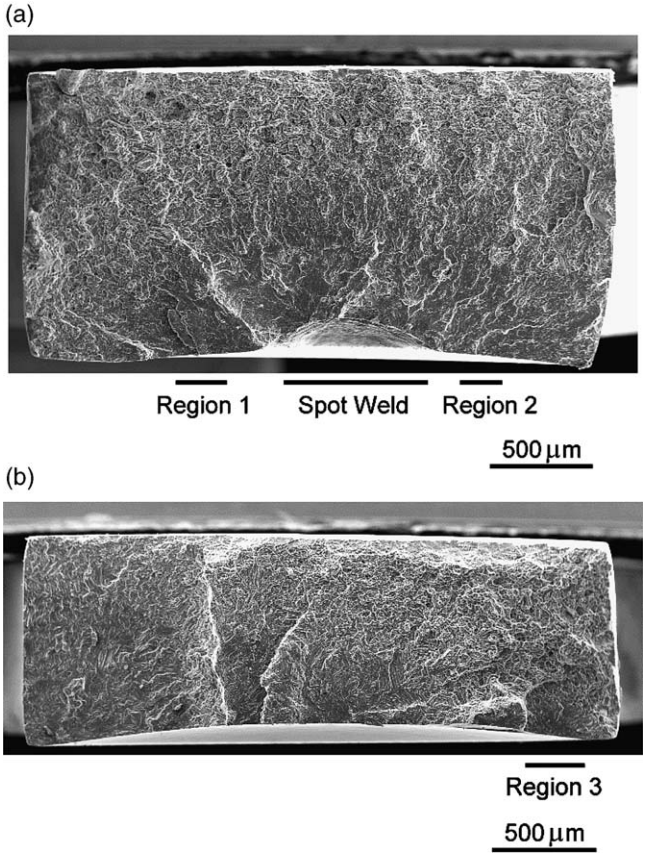

Fig. 2. SEM images of the fracture surface from the tests in (a) vacuum and (b) water vapor. Several positions that were inspected in-situ during fatigue are indicated below the respective images.

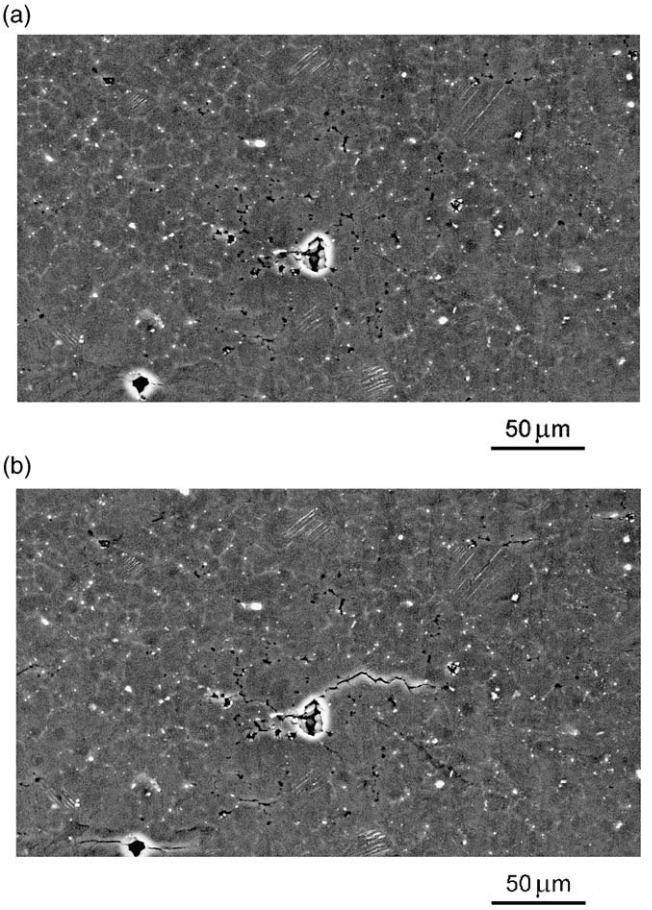

Fig. 3. Fatigue crack formation in Region 1 in the sample tested in a vacuum at (a) 3200 and (b) 7300 cycles.

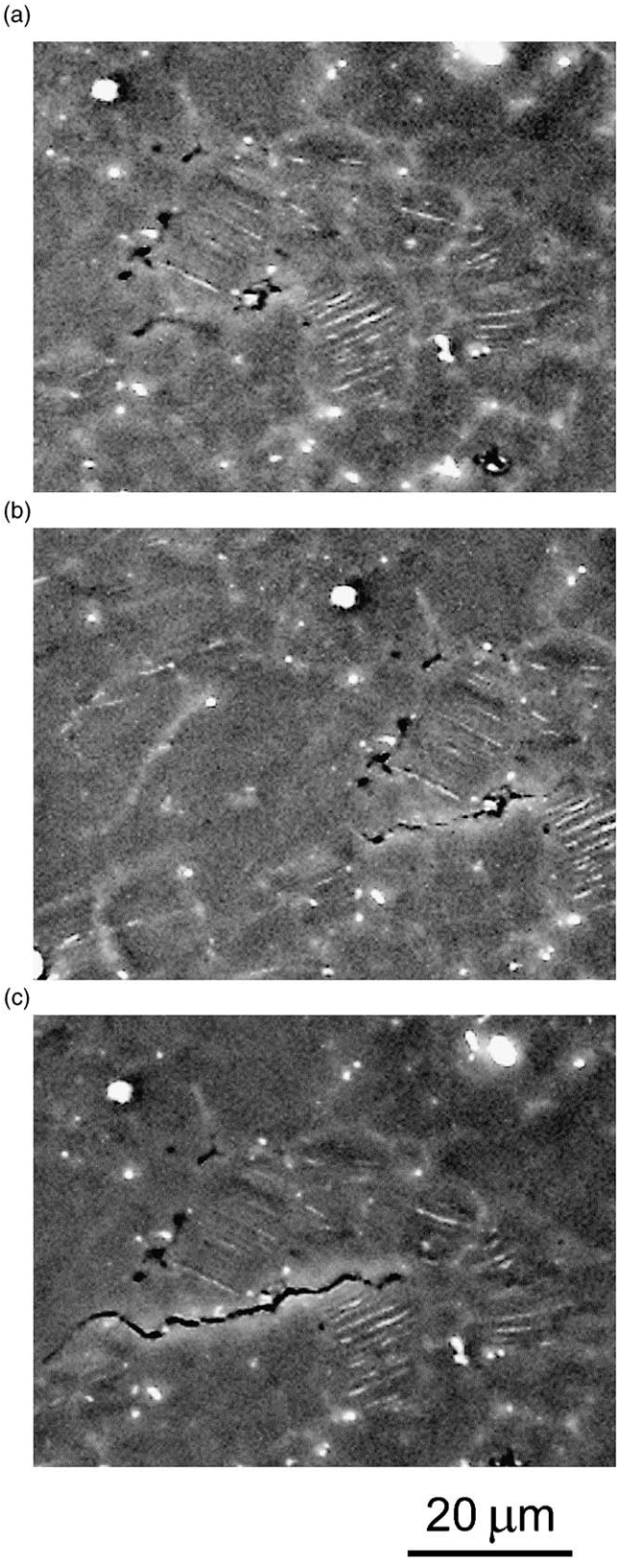

Fig. 4. Fatigue crack formation in Region 2 in the sample tested in a vacuum with porosity at (a) 3200, (b) 4000, and (c) 7300 cycles.

3a and b we observe the formation of three different cracks in the vacuum environment between cycles (a) 3200 and (b) 7300 in a region with a rather high volume fraction of microporosity (small black spots) surrounding a large pore (Region 1). In the lower left of Fig. 3a, a small crack has initiated on the right side of the pore by cycle 3200. The pore in the center also has a small crack on its left side by 3200 cycles. Also note that the large α-Mg dendrite cell in the upper right has a few persistent slip bands, but no cracks at 3200 cycles (Fig. 3a). At 7300 cycles (Fig. 3b), a rather large crack has formed on the right of the center pore, and the pore on the lower left also has cracks emanating from both sides. The intersection point between the persistent slip band in the large dendrite on the upper right and some local porosity has also formed a small crack sometime before 7300 cycles. *None of these features existed after the pre-cycling history of 130 cycles at 135 MPa.*

In Fig. 4 we examine another crack formation event under vacuum in a porous region (Region 2) with a smaller volume fraction of porosity at the surface. At 3200 cycles (Fig. 4a) the crack is not seen at the scale of observation, but numerous persistent slip bands are evident in adjacent dendrite cells. Approximately 800 cycles later (Fig. 4b), a small crack has formed in the interdendritic region by linking small pores at the surface. After 7300 cycles (Fig. 4c) the crack has grown to an appreciable size. Clearly, the driving force for the formation of the crack in Fig. 4 is the strong slip incompatibility between adjacent grains as marked by the presence and absence of persistent slip bands. Under vacuum, cracks were also observed to form in the base Mg material rather than at a pore or within the interdendritic region. In Fig. 5 we track the development of a fatigue crack at persistent slip bands within a rather large dendrite cell. The persistent slip bands coarsen as a function of cycling until a crack is distinctly formed between 11,000 (Fig. 5c) and 15,700 cycles (Fig. 5d). The precise cycle at which the crack formed is vague, but it is certain that the crack in Fig. 5c took longer to initiate (between 11,000 and 15,700 cycles) compared to the cracks at the pores in Figs. 3 and 4 (between 3200 and 7300 cycles).

Figs. 6–8 present observations of the propagation of small fatigue cracks during cycling at 90 MPa in the vacuum environment. Fig. 6 shows a series of images tracking the progression of the crack formed at the center pore in Fig. 3 (Region 1). In only 11,000 cycles, the crack has progressed through the region of high microporosity (Fig. 6b). Following initial propagation through the porosity-laden interdendritic network, by a distance of about 6–10 times the average dendrite cell size, the crack grows straight in a direction roughly perpendicular to the loading axis on both sides (Fig. 6c-e). The crack on the left of the pore ultimately takes a significant turn only to merge with a region containing a microcrack. A slightly different growth pattern is

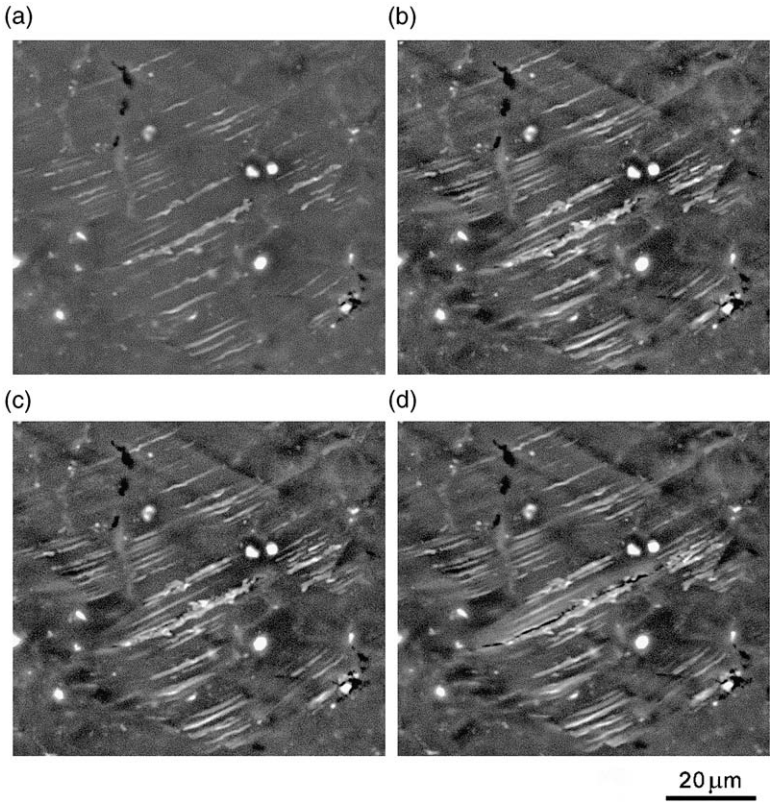

Fig. 5. Fatigue crack formation within a large dendrite cell in the sample tested in a vacuum at persistent slip bands at (a) 3200, (b) 7300, (c) 11,000, and (d) 15,700 cycles.

observed for the small crack formed in Region 2, as shown in Fig. 7. The crack in Fig. 7b is considerably smaller than the crack in Fig. 6b at equivalent cycle numbers. Although the crack in Fig. 7 does not have an extensive micro-porosity network to travel through during the initial stages of growth, the crack still meanders significantly through the microstructure. The meandering is linked to propagation along persistent slip bands in dendrite cells and in interdendritic regions. In fact, multiple observations of small and large fatigue cracks following persistent slip bands ahead of the crack tip were made in the vacuum environment. Fig. 7 also indicates that propagation occurs in part along interdendritic regions between misoriented cells (PSBs in different directions or PSBs occurring in one cell and not its neighbors), again likely due to incompatibility of slip for the low symmetry HCP lattice.

Fig. 8 presents images from the specimen tested in vacuum, i.e. the left half of the crack seen in Fig. 6 from Region 1. The image in Fig. 8a was created using secondary electrons, while high-contrast backscatter electron imaging created the image in Fig. 8b. The purpose of Fig. 8b is to generally show the location of microstructural features relative to the crack path, while Fig. 8a shows a duplicate high-resolution image of the crack. Although the crack initially follows the interdendritic region with microporosity, it eventually propagates through the dendrite cells when it has a *half-length* roughly 3–5 times the average dendrite cell size. Small kinks in the crack growth direction seen in Fig. 8a are linked to the impingement of the crack on interdendritic boundaries, the bright areas in Fig. 8b. However, crystallographically favored crack paths cause larger changes in the growth direction of the cracks (Fig. 7). Fig. 9 presents a final set of images from Region 1 showing (a) the fracture surface top-view and (b) an in situ view after final fracture. Aside from the major pore and surrounding micropores that promoted crack formation, minimal porosity was detected on the fracture surface in Region 1. Similarly, minimal porosity was discovered on the fracture surface in Region 2. Consequently, we can eliminate the possibility that a large pore hidden underneath the surface formed the crack that was examined in situ at the surface.

In situ SEM images from the sample fatigued in the water vapor environment are shown in Figs. 10–13. Fig. 10a shows a small crack that formed within a dendrite cell in the cast Mg after 100 cycles at 135 MPa. Similar cracks were *not found* in the sample cycled in vacuum after 130 cycles at 135 MPa. Fig. 10b shows the same crack after 11,000 cycles at 90 MPa, with a slightly shifted field of view. The small crack follows a predominant Mode I growth pattern through the dendrite cells, changing direction only when encountering an AlMnSi

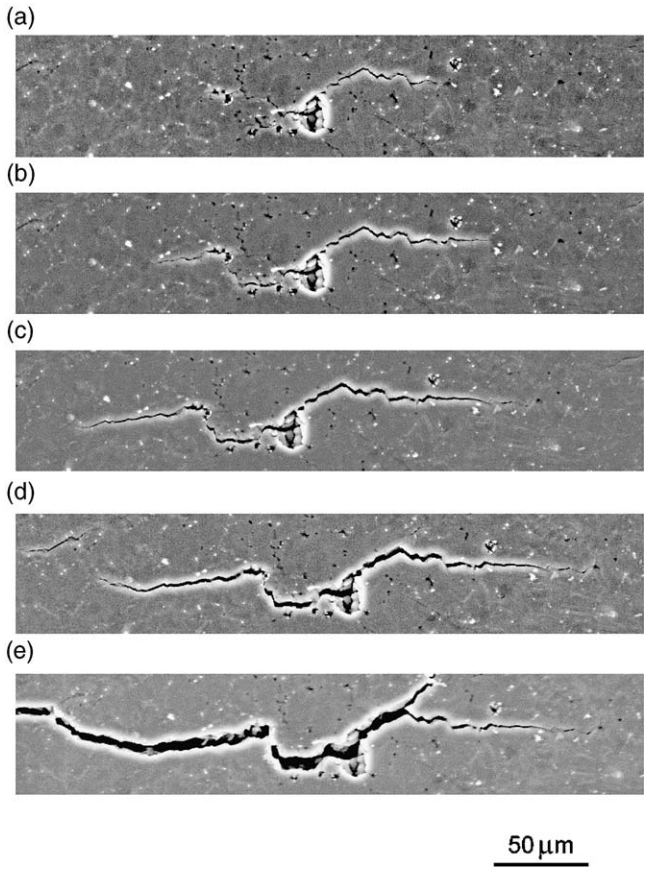

Fig. 6. Propagation of a small fatigue crack from a pore in Region 1 in the sample tested in vacuum at (a) 7300, (b) 11,000, (c) 19,300, (d) 22,600, (e) and 34,813 cycles.

particle (Fig. 10b). Fig. 11 shows a small crack formed by the linking of microporosity at (a) pre-cycling and (b) 11,000 cycles at 90 MPa in Region 3 (Fig. 2b). The crack is initially formed in a region of microporosity, and it grows both through the dendrite cells and in the interdendritic regions. The crack does not closely follow the micropores in adjacent dendrite cells. Fig. 12 compares a typical crack in the cast magnesium alloy cycled in (a) vacuum and (b) water vapor environments, at 34,000 and 11,000 cycles, respectively. The crack in Fig. 12a is about 300 μm long, while the crack in Fig. 12b has a total length of about 250 μm. Despite similar microstructures, the fatigue crack in the magnesium cycled in vacuum interacts more strongly with the microstructure, as evidenced by its prolonged meandering, compared to the crack in the magnesium cycled in water vapor. Fig. 13 is an image of the fracture surface from Region 3 (Figs. 2b and 11). The fracture surface shows negligible porosity away from the initiation site and highlights different regions of crack growth behavior (note the semicircular crack path).

Fig. 14 presents crack size as a function of cycle number for various cracks in water vapor and vacuum. The purpose of Fig. 14 is to demonstrate the difference in

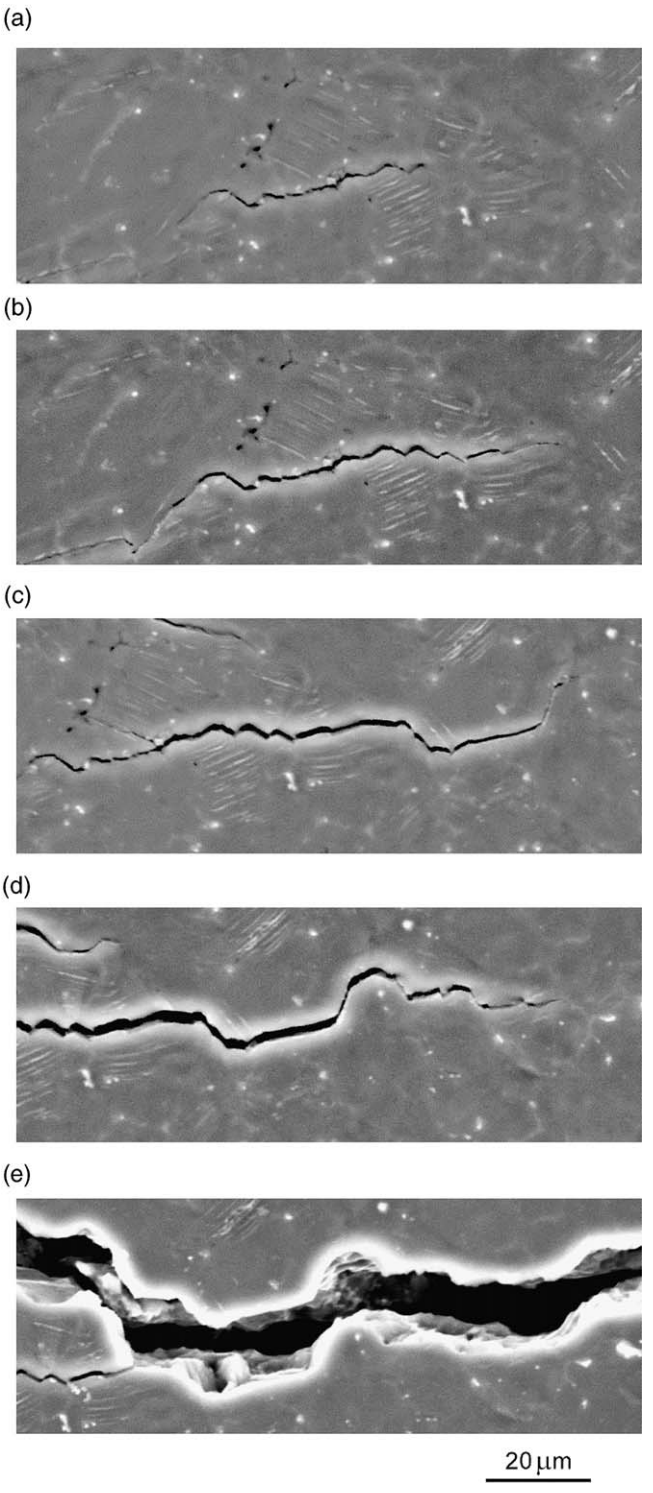

Fig. 7. Propagation of a small fatigue crack through the microstructure in Region 2 in the sample tested in vacuum at (a) 7300, (b) 11,000, (c) 19,300, (d) 22,600 cycles, and (e) 34,813 cycles.

"average" crack growth rate of cracks growing in water vapor versus vacuum. For all cracks observed, on average, the cracks grow faster in the water vapor versus vacuum. The details of this observation will depend on the applied loading conditions, absolute crack size, and

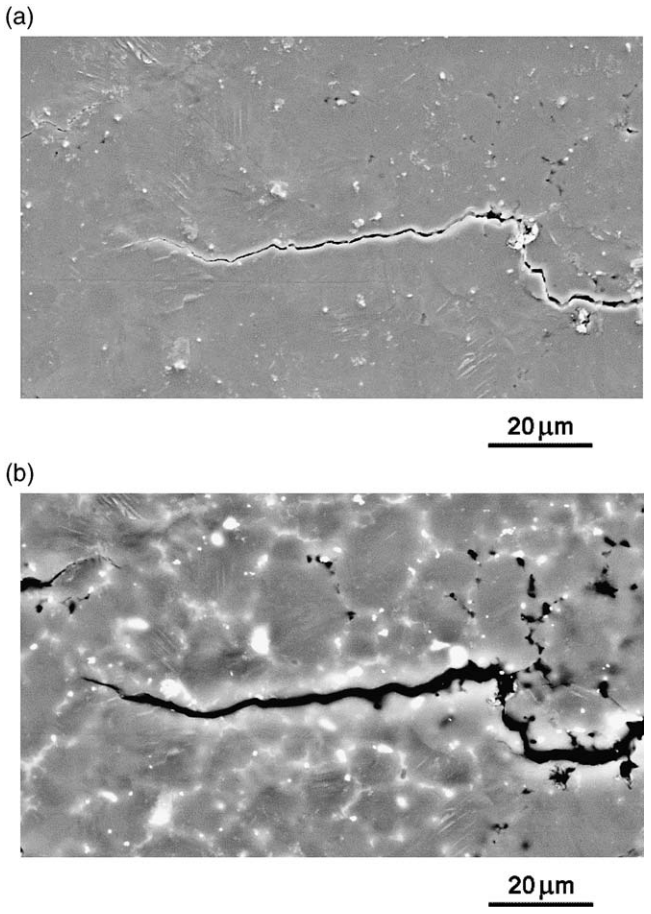

Fig. 8. Higher magnification view of the left half of the crack in Fig. 6d in Region 1 in the sample tested in vacuum. The crack was imaged using (a) secondary and (b) backscatter electrons.

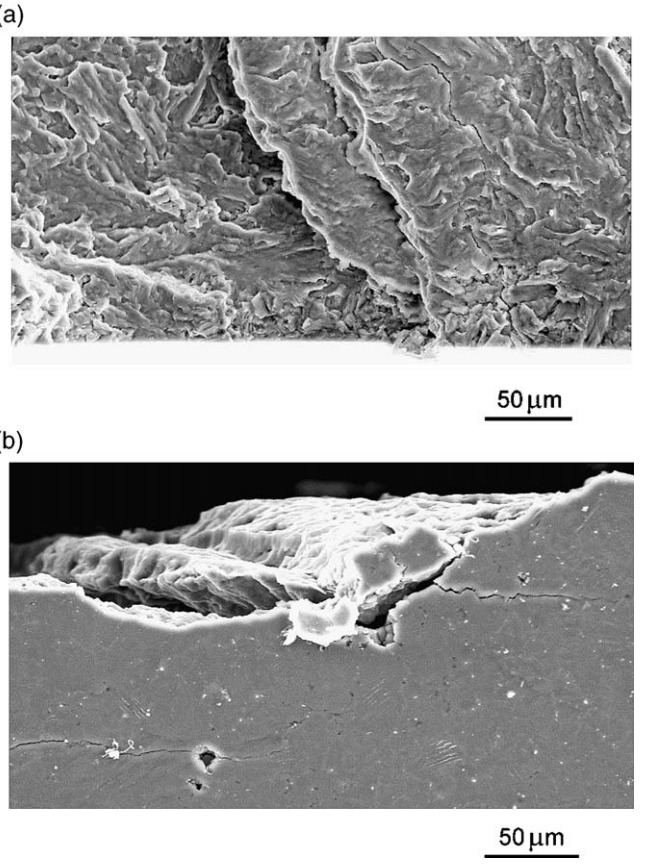

Fig. 9. Post-mortem view of the crack in Region 1 in the sample tested in vacuum from the (a) fracture surface and (b) in-situ viewing plane.

local microstructural conditions. In the present work, we have not tracked the cracks at frequent cycle intervals as needed to report more detailed crack growth rate data. However, the data in Fig. 14 is sufficient to demonstrate that the average crack growth rate of cracks in water vapor is higher than those in vacuum for the crack sizes examined.

4. Discussion

The purpose of this paper is to provide a qualitative assessment of the fatigue mechanisms in cast AM60 Mg using in situ environmental SEM microscopy. Particular emphasis is placed on examining the early stages of fatigue, including crack formation and microstructurally small crack propagation. In this discussion we will first assess the observed mechanisms in the context of relevant literature, then we will consider the impact of the observations on micro-mechanical modeling of fatigue mechanisms. Before discussing the results we note that caution should be exercised when interpreting surface observations in terms of fatigue mechanisms. It is always

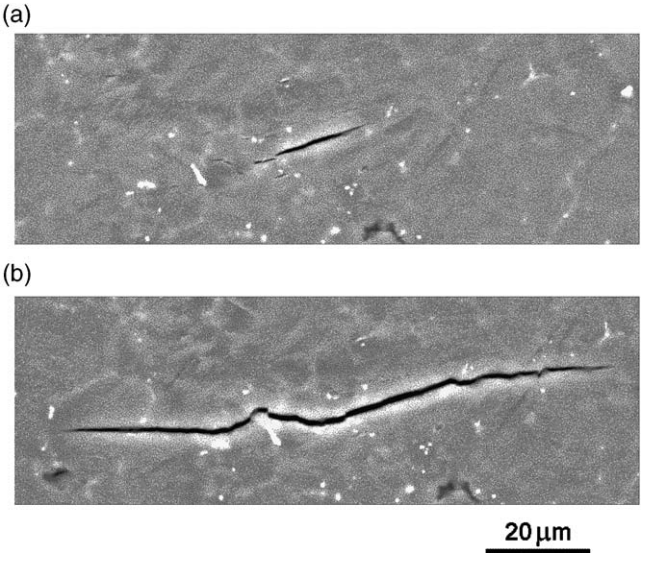

Fig. 10. Cracks in the specimen cycled in water vapor after (a) precycling and (b) 11,000 cycles.

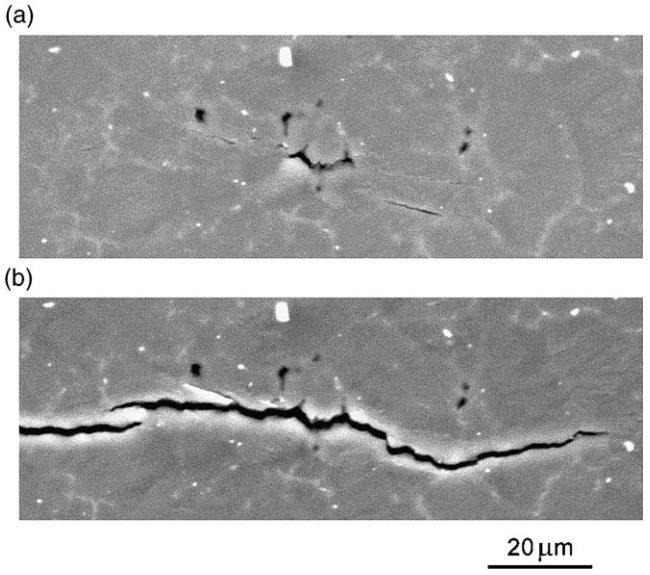

Fig. 11. Cracks in the specimen in cycled water vapor in Region 3 after (a) pre-cycling and (b) 11,000 cycles.

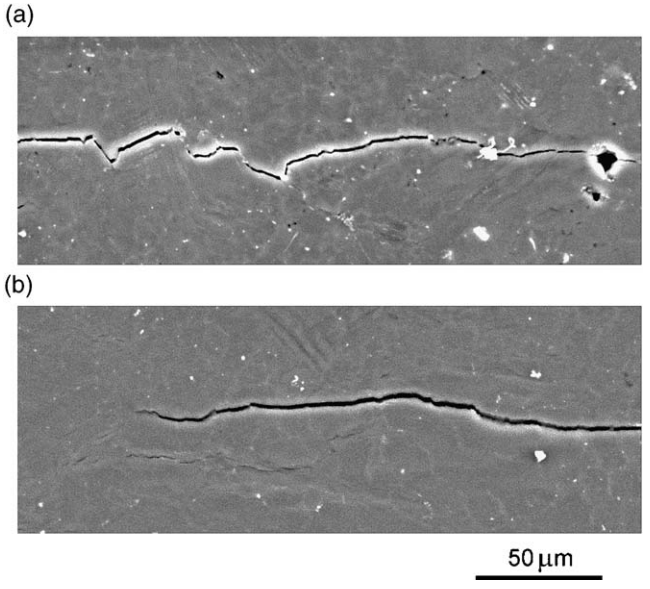

Fig. 12. Comparison of crack profiles in a cast magnesium alloy under the following conditions (a) vacuum at 34,000 cycles and (b) water vapor at 11,000 cycles.

possible that the observed damage may only be present at the surface. In all cases we have attempted to find cracks with relatively large opening displacements at maximum load, such that they likely extend reasonably into the bulk microstructure. Nearly all of the results presented here represent significant cracks that contributed to the final fracture path. For example, the crack monitored in Region 3 showed a relatively fast surface growth rate (Fig. 11), but also showed proportional penetration into the bulk material via post-mortem fractography (Fig. 13).

In the present study we have observed in situ the formation of fatigue cracks at casting pores in a vacuum environment (Figs. 3 and 4) and a water vapor environment (Fig. 11). In the vacuum environment, some cracks formed after very few cycles at 10–20 micron pores without appreciable accumulation of cyclic plasticity, via persistent slip band formation, in the surrounding dendrite cells (Fig. 3). However, we also observed crack formation under vacuum in a region with smaller micropores (2–4 microns) that was preceded by an observable accumulation of cyclic plasticity in the surrounding dendrite cells (Fig. 4). The existence of *local* plastic strain accumulation via persistent slip bands in the relatively small dendrite cells in Fig. 4 was uncommon. However, the cyclic plasticity was clearly linked to the presence of porosity coupled with the favorable shearing orientation of primary slip systems in the dendrite cells with respect to the loading axis (approx. 45° angle to the applied loading direction). It is important to note the significant slip incompatibility observed in adjacent dendrite cells near the crack initiation site in Fig. 4. The presence of slip in some cells and the absence

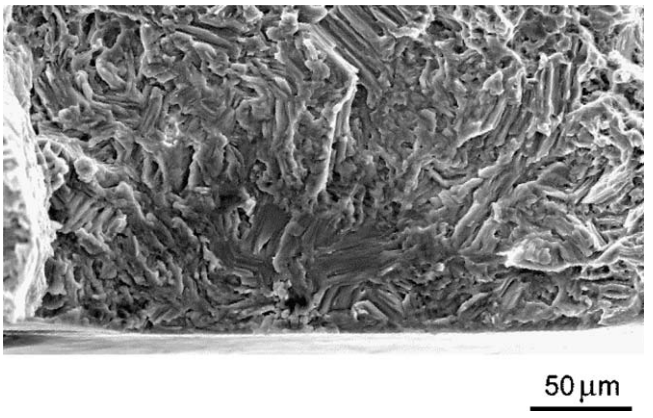

Fig. 13. Image from the fracture surface of the specimen in Region 3 from the sample tested in water vapor.

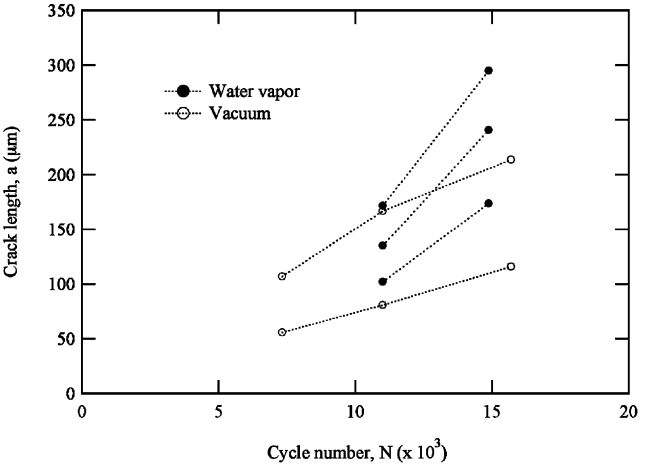

Fig. 14. Snapshot of crack size as a function of cycle number for several cracks growing in vacuum versus water vapor.

of slip in others, leads to strong plastic strain mismatches and high stresses in the interdendritic regions. All of these factors contributed to the formation of a fatigue crack in this interdendritic region. A previous study [24] has also observed slip features near sites of crack formation in extruded Mg via a post-mortem fracture analysis. In the water vapor environment, cracks started near pores without observable persistent slip band formation (Fig. 11).

Fatigue cracks were also found to form within large, relatively soft α-Mg dendrite cells in vacuum (Fig. 5) and water vapor (Fig. 10) environments. In the vacuum environment, the crack formation was evident at persistent slip bands within relatively large dendrites that are favorably oriented with respect to the loading axis. The large dendrite cell in Fig. 5 is nearly 60 μm in diameter, compared to an average cell size of 10 μm near the nucleation site in Fig. 4. Persistent slip band formation and subsequent local surface roughening, as a function of cycles, was frequently observed in large dendrite cells. The extrusions and intrusions at the surface eventually lead to fatigue crack formation as typical for wrought materials. It is interesting that once formed, the crack rapidly reaches the size of the dendrite cell by spanning the weakened shear zone (Fig. 5). In the vacuum environment, the crack formation life for this mechanism is significantly longer than the formation life near pores. However, if the maximum pore size in a highly stressed region is reduced below a critical level, this traditional persistent slip band mechanism may dominate if large dendrite cells are present.

In contrast to observations in the vacuum environment, crack formation in the water vapor environment was relatively rapid in selected regions without noticeable influence of surrounding porosity. Fig. 10 shows an example of a fatigue crack that formed in the water vapor environment during precycling. Several similar cracks rapidly formed in the Mg cycled in water vapor that were not connected with porosity or observable persistent slip bands. Apparently, the water vapor accelerates the fatigue crack formation process in the Mg in specific locations. This acceleration of fatigue crack formation does not occur at all microstructural features in the sample, as evident from the smaller total number of cracks growing in the sample cycled in the water vapor environment. However, in selected locations, cracks formed faster in the water vapor environment. We note that relatively large pores, which usually exist in the interior of a larger component, might still facilitate early crack formation compared to traditional surface mechanisms. However, such pores did not exist in this die-casting, and in addition these pores will not be subject to the environmental effects noted here.

Based on crack tip stresses, cracks should preferentially grow in a Mode I direction. However, particularly for microstructurally small cracks, variations in the microstructure can alter the direction of crack growth in an effort to avoid an obstacle or link with a weakened material zone. In the water vapor environment, microstructurally small surface fatigue cracks in the cast magnesium alloy preferentially propagated straight through the dendrite cells. Some crack meandering through the microstructure was discovered when the cracks would propagate through interdendritic regions. However, the meandering of the cracks growing in the water vapor environment was minimal compared to the meandering of the cracks in the vacuum environment. In the presence of the harsh environment, nominally Mode I growth through the dendrite cells was accelerated. The cracks formed in the water vapor environment were only noticeably deterred from straight Mode I growth patterns by interdendritic regions (Fig. 11) or second phase particles (Fig. 10). In addition, small fatigue cracks did show some meandering to link with other micro cracks in the near vicinity (Fig. 11). Meandering is evident from the linkage of the main crack (Fig. 11b) and a small crack to the lower right of the formation site (Fig. 11a).

In the vacuum environment, microstructurally small fatigue cracks grew through the dendrite cells, persistent slip bands, and interdendritic regions. Fatigue cracks growing in the vacuum generally grew much more slowly, i.e., more cyclic damage was required to accumulate ahead of the crack tip (Fig. 14). Previous studies have shown that long fatigue cracks grow more slowly in lower humidity environments [13,14]. The small fatigue cracks in the vacuum environment were found to propagate preferentially through persistent slip bands formed ahead of the crack tip as has been previously observed in cast Mg [18] and other alloys [25]. Fatigue cracks prefer to propagate along the persistent slip bands because these regions have been weakened by intense dislocation activity and cracking. Fatigue cracks prefer to grow along interdendritic regions when micropores are present to help create a weak crack path (Fig. 6). In addition, small cracks can propagate in or near the interdendritic regions when slip incompatibility between cells generates high stresses in the interdendritic regions (Fig. 7).

In previous work we have observed that a fatal internal crack, as observed post-mortem on the fracture surface, prefers to propagate through the Mg dendrite cells at small sizes [17]. Based on the present observations in vacuum and water vapor, we see that this tendency is amplified in the presence of environmental effects. The rationale is that small cracks have a relatively more difficult time propagating through interdendritic regions which contain β particles within a Mg matrix with high levels of Al in solid solution that is relatively stronger then the interior of the dendrite cells. The small fatigue cracks, with very small crack tip plastic zones, prefer to propagate through the relatively soft α-Mg cells. However, the presence of microporosity in

the interdendritic regions amplifies the crack tip driving force and cracks in vacuum have been observed to move along interdendritic regions, propagating through these micropores. In addition, the crack tip driving force may be significantly amplified near the interdendritic regions by slip incompatibility between the α-Mg cells. This amplification can cause small cracks to propagate in or near the interdendritic regions where incompatibility of slip is highest.

Micro-mechanical modeling of these phenomena using the finite element method will provide more quantitative information for larger scale modeling efforts and casting design guidelines. Any model that hopes to capture the relevant physics of the problem should account for the low symmetry slip anisotropy in HCP Mg and the effects of the periodic interdendritic regions. Fatigue crack formation and small crack propagation, without environmental influence, is highly dependent on preferential basal slip in α-Mg. This preferential slip can lead to slip incompatibilities between cells and persistent slip bands within cells, both of which are critical for crack formation and small crack propagation. The influence of the environment on the formation and growth of surface cracks also appears to be of significant importance. Based on the present results, introduction of a water vapor environment reduces the resistance to fatigue crack formation and growth in cast Mg. Because of this, rapidly propagating cracks do not meander onto crystallographic planes as often as cracks that are slowly propagating without environmental influence. The presence of the environment weakens the dendrite cell material's inherent resistance to fatigue crack propagation. One possible rationale for this would be hydrogen embrittlement due to the reaction of water vapor with freshly exposed material at the crack tip. However, at present this mechanism is speculative and needs more study. Modeling of this environmental effect may involve a relative weakening of the fatigue resistance of the dendrite cell as a function of environment.

The effect of different local cyclic plasticity levels in the Mg grains near pores needs quantification. Cyclic plastic strain levels necessary to form a fatigue crack may depend on the orientation of the grains near the pores, and the relative size of the dendrite cells and pores. Both large dendrite cells and large pores elevate *local* cyclic plasticity levels. Similarly, the effect of the interdendritic regions on crack propagation needs further quantification with modeling. In the presence of porosity or slip incompatibility, the cracks seem to select the interdendritic regions for growth. However, in some situations, the cracks avoid these regions and grow through the dendrite cells. Clearly, accurate micromechanical models are needed to examine the effect of the Al-rich and β particle-laden interdendritic architecture on small crack growth driving forces. However, more experimental work is required to shed light on the relative strength of these regions as barriers to small crack growth. This could come from quantitative small crack growth studies supplemented by large crack studies on Mg materials with different Al contents, and perhaps nanoindentation.

5. Conclusions

1. The presence of a water vapor environment significantly alters the nucleation and small crack propagation characteristics and rates in cast AM60 Mg compared to a vacuum environment.
2. In a vacuum environment, surface fatigue cracks formed rapidly at larger pores, sometimes preceded by observable cyclic slip accumulation. At higher cycle numbers in the vacuum environment, additional cracks were discovered to form at persistent slip bands within relatively large dendrite cells.
3. In a vacuum environment, microstructurally small fatigue cracks were found to follow interdendritic regions in the presence of a high level of microporosity and crystallographic planes in the presence of persistent slip bands ahead of the crack tip. In the absence of these weak microstructual paths, small cracks propagated straight through the dendrite cells and in, or near, interdendritic regions, depending on the local cell arrangement.
4. In a water vapor environment, isolated surface cracks formed rapidly within the Mg cells and at pores. Small cracks in the magnesium cycled in water vapor grew significantly faster than in the vacuum. Small fatigue cracks in the magnesium cycled in water vapor often propagated straight through the dendrite cells in a Mode I manner. The cracks in the water vapor environment sometimes propagated in, or near, interdendritic regions, but less often compared to cracks growing in the vacuum environment.
5. Small fatigue cracks in the magnesium avoided second phase particles in both vacuum and water vapor environments. The interdendritic regions also caused perturbations in fatigue crack paths in both water vapor and vacuum environments.
6. The effect of porosity on the fatigue mechanisms in cast Mg depends on the relative size and distribution of the pores. Distributed microporosity (1–2 microns) caused a preferential path for small fatigue cracks. Slightly large micropores (10–20 microns) served as crack formation sites.
7. The growth pattern of small cracks ($a < 6$-10DCS, where DCS is the average dendrite cell size) was more sensitive to microstructural features in the cast Mg compared to the predominantly Mode I growth pattern of cracks longer than about 6–10 DCS.

Acknowledgements

The authors thank Anja Puda for her careful surface preparation of the cast Mg alloy specimens for in situ studies. This work was sponsored by the US Department of Energy under contract DE-AC04-94Al85000, and was performed with the support of Dick Osborne and Don Penrod for the USCAR Lightweight Metals Group. Funding for K. Gall was provided by a DOE PECASE award from Sandia National Laboratories.

References

[1] Jambor A, Beyer M. Mater Des 1997;18:203–9.
[2] Froes FH, Eliezer D, Aghion EL. JOM 1998;50:30–4.
[3] Makar GI, Kruger J. Int Mater Rev 1993;38:138–53.
[4] Alves H, Koster U, Aghion E, Eliezer D. Mater Tech 2001;16:110–26.
[5] Lunder O, Aune TK, Nisancioglu K. Nat Ass Corr Eng 1987;43:291–5.
[6] Song G, Atrens A, Dargusch M. Corros Sci 1999;41:249–73.
[7] Ambat R, Aung NN, Zhou W. Corros Sci 2000;42:1433–55.
[8] Ghali E. Mag Alloys 2000. Mater Sci Forum 2000;350:261–72.
[9] Gray JE, Luan BJ. Alloy Compos 2002;336:88–113.
[10] Perov SN, Ogarevic VV, Stephens RI. J Eng Mater Tech 1993;115:385–90.
[11] Goodenberger DL, Stephens RI. J Eng Mater Tech 1993;115:391–7.
[12] Stephens RI, Schrader CD, Lease KB. J Eng Mater Tech 1995;117:293–8.
[13] Shibusawa T, Kobayashi Y, Ishikawa K. J Jap Inst Met 1997;61:298–302.
[14] Fuchs U, Lipowsky H, Mayer H, Papakyriacou M, Stich A, Tschegg S, Zettl B. Mat Wiss Werk 2002;33:15–23.
[15] Mayer HR, Lipowsky H, Papakyriacou M, Rosch R, Stich A, Stanzl-Tschegg S. Fatigue Fract Eng Mater Struct 1999;22:591–9.
[16] Fuchs U, Lipowsky H, Mayer H, Papakyriacou M, Stich A, Tschegg S, Zettl B. Mat Wiss Werk 2002;33:117–27.
[17] Horstemeyer MF, Yang N, Gall K, McDowell DL, Fan J, Gullet P. Fatigue Fract Eng Mater Struct 2002;25:1–12.
[18] Eisenmeier G, Holzwarth B, Höppel HW, Mughrabi H. Mater Sci Eng A 2001;319:578–82.
[19] Stephens RI, Grabowski L, Hoeppner DW. Int J Fatigue 1993;15:273–82.
[20] Halliday MD, Poole P, Bowen P. Fatigue Fract Eng Mater Struct 1995;18:717–29.
[21] Halliday MD, Zhang JZ, Poole P, Bowen P. Int J Fatigue 1997;19:273–82.
[22] Zhang XP, Wang CH, Chen W, Ye L, Mai YW. Scripta Mater 2001;44:2443–8.
[23] Li WF, Zhang XP. Mater Sci Eng A 2001;318:129–36.
[24] Shih TS, Liu WS, Chen YJ. Mater Sci Eng A 2002;325:152–62.
[25] Halliday MD, Poole P, Bowen P. Mater Sci Tech 1999;15:382–90.